Late Holocene paleoseismology of the Kenai Peninsula and Kachemak Bay region, Alaska and implications for plate segmentation

External Grant Award # G13AP00051

Investigators: Ian Shennan, Natasha Barlow and Ed Garrett

Sea Level Research Unit
Department of Geography
University of Durham
Durham
DH1 3LE
United Kingdom

Tel: +44 191 334 1934
Fax: +44 191 334 1801
Email: ian.shennan@durham.ac.uk
URL: http://www.geography.dur.ac.uk

Start date: July 1st 2013
End date: June 30th 2014

Key words: Paleoseismology, Recurrence interval, Surface deformation

Research supported by the U.S. Geological Survey (USGS), Department of the Interior, under USGS award number **G13AP00051**. *The views and conclusions contained in this document are those of the authors and should not be interpreted as necessarily representing the official policies, either expressed or implied, of the U.S. Government.*

© I Shennan, N Barlow and E Garrett 2014

Abstract

We sampled five sites: Beluga Slough and Beluga Wetlands at Homer; Kasilof River; and Peterson Bay and Sadie Cove on the south shore of Kachemack Bay, using outcrops and hand driven cores to determine the lateral continuity of sediment layers prior to selecting which samples to return to Durham. We collected new modern surface sediment samples from Beluga Slough to extend the modern diatom database for south central Alaska and develop a new suite of diatom based transfer function models. We obtained 21 new AMS radiocarbon dating results.

The most comprehensive records of relative land and sea-level changes come from Beluga Slough, Homer, with a >4000 year record, and Kasilof, a >6000 year record. Very few of the peat-mud couplets fulfil the criteria for recording coseismic deformation. We conclude that no previous great earthquake in the last few thousand years showed the same spatial pattern of deformation as 1964. Along the west coast of the Kenai Peninsula, a great earthquake c. 1500BP produced more subsidence than in 1964, whereas all the other prehistoric earthquakes produced limited or no evidence of coseismic deformation at Kenai, Kasilof and Homer.

We find no evidence for tsunami deposits at Homer and Kasilof.

Evidence from Kenai, Kasilof and Homer suggest that spatial variations seen in the present-day slip deficit distribution in some way relate to characteristics of the subduction fault that impact through the coseismic and interseismic phases of multiple earthquake cycles. We should consider whether the patterns of coseismic deformation for the last few thousand years reflect a mosaic of stronger and weaker patches. For example, the Prince William Sound segment would be an area of closely placed stronger patches, with the subduction interface characterised by the flat slab subduction of the Yakutat slab. Kenai, Kasilof and Homer would lie in a region of more widely spaced asperities and areas of aseismic slip; and Kodiak would be another area of closely spaced stronger patches.

Context

This proposal set out to undertake new field and laboratory investigations and subsequent data analyses to examine geologic evidence of Holocene ground displacements and tsunami sedimentation in the Kenai Peninsula (from Kasilof River to Homer) and Kachemak Bay, Alaska, associated with past subduction zone earthquakes. It builds on previous work undertaken by the principal investigators elsewhere in Alaska and the Pacific Northwest, together with the development of diatom transfer functions to quantify relative land and sea-level changes. Our published investigations quantify vertical ground displacements affecting upper Cook Inlet for seven great earthquakes during the last 4000 years. Beyond upper Cook Inlet the broader spatial pattern of co-seismic and interseismic deformation is not known for most of these events and is poorly quantified for all except 1964. Thus, we do not yet know whether the spatial pattern of vertical deformation observed for each event is the same or different. This limits our ability to test models of plate boundary rupture and segmentation that require spatial data regarding relative land and sea-level data over multiple events. These models are key to assessing future seismic hazard in Alaska and on other plate boundaries.

We set out four research questions:

1. Can we quantify geologic estimates of land-level changes from great Holocene plate boundary earthquakes and complete earthquake cycles across three sites in the Kenai Peninsula – Kachemak Bay region?
2. Is there evidence of Late Holocene earthquake-generated tsunami?
3. How do spatial patterns of estimated land-level changes for different Holocene plate boundary earthquakes vary between Kodiak Island and western Yakataga?
4. Are great earthquake ruptures in Alaska controlled by persistent segment boundaries or do the rupture areas overlap?

Anticipated deliverables were:

1. Collection of cores or sampling of exposed sections to examine possible earthquake horizons at 3 sites – Kasilof River, Homer and the south shore of Kachemak Bay;
2. Analysis of fossil diatom samples;
3. Application of transfer function models to quantify geological estimates of land-level changes;
4. Analysis of AMS dated *in situ* macrofossils to provide a chronology of late Holocene great earthquakes in south central Alaska and correlations between Kodiak Island, Cook Inlet, Copper River Delta, Cape Suckling/Bering Glacier, Yakataga coast;
5. Evaluation of the patterns of pre-1964 co-seismic deformations;
6. Presentation of results at scientific meetings;
7. Submission of results to an international refereed journal.

1 Summary of deliverables

We sampled five sites: Beluga Slough and Beluga Wetlands, at Homer; Kasilof River; and Peterson Bay and Sadie Cove on the south shore of Kachemack Bay (Figure 1). We used both outcrops and hand driven cores to determine the lateral continuity of sediment layers prior to selecting which samples to return to Durham. Beluga Slough is a tidal marsh protected from the open coast by a sand and gravel beach ridge, in contrast to the more open geomorphic settings of most other sites studied to date. Therefore, we collected new modern surface sediment samples from Beluga Slough to extend the modern diatom database for south central Alaska and develop a new suite of diatom based transfer function models. Laboratory analysis focuses on diatom analysis of the modern and fossil sediments and radiocarbon dating. We obtained 21 new AMS radiocarbon dating results. We discuss these data and their correlation with the broader region of the 1964 rupture zone. We presented preliminary findings at SSA 2014 and IGCP 588 2014. We shall submit a paper to a journal late 2014.

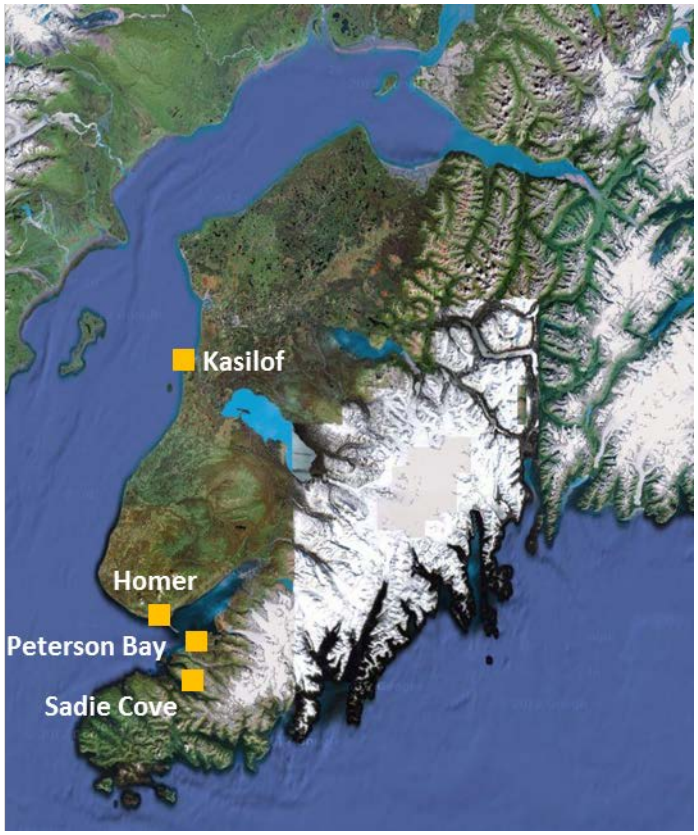

Figure 1: Location of sites

2 Results

2.1 Research Question 1. Can we quantify geologic estimates of land-level changes from great Holocene plate boundary earthquakes and complete earthquake cycles across three sites in the Kenai Peninsula – Kachemak Bay region?

2.1.1 Methods and revised diatom transfer function models

For the diatom analyses presented, we use quantitative methods using transfer function approaches, developed and successfully applied at other sites in south central Alaska (Shennan et al., 2014b; Shennan et al., 2014c). For the transfer function models we use a regional-scale modern training set collected from a wide range of marshes across ~1000 km of south central Alaska in order to seek the best fit between fossil and modern diatom assemblages (Watcham et al., 2013). Beluga Slough, Homer is a tidal marsh protect from the open coast by a sand and gravel spit that reduces the tidal influence according to the geometry of the channel through the spit. This is the first modern marsh that we have sampled with such a morphology, therefore we collected new modern sediment samples to enlarge the database for fossil reconstructions. We use three models, constrained by the lithology of the Holocene sediment sequence; one for peat sediment, a second for organic silt units and silt units with visible plant rootlets, and a third for silt units with no rootlets (Hamilton and Shennan, 2005a; Shennan et al., 2014b). We assess goodness of fit between each fossil sample and the modern dataset with a dissimilarity coefficient, using the 20th percentile of the dissimilarity values for the modern samples as the cut-off between 'close' and 'poor' modern analogues for fossil samples, and the 5th percentile as the threshold

for defining 'good' modern analogues. For reconstruction of the elevation at which the fossil sediment accumulated, termed paleomarsh surface elevation, we present sample-specific 95.4% (2σ) error terms.

The addition of new modern samples from Beluga Slough to the transfer function reinforces a methodological debate that we raised previously (Barlow et al., 2013; Watcham et al., 2013). A modern dataset dominated by modern samples from the local site, i.e. in the same marsh or estuary as the fossil core, will most likely provide the smallest error terms for the youngest samples. In contrast, it is may not provide good analogues for older samples. By definition, all our modern samples are from the post-seismic period of the latest earthquake deformation cycle; therefore, we see no a priori reason to suppose that a local dataset will provide all modern analogues for our fossil sequences that may be thousands of years older and from different phases of an earthquake cycle. The first effect of increasing the sample size to include Beluga Slough increases the model error terms for RSL reconstructions (Table 1). The largest increase is within the upper elevation range, demonstrated in model 1, and reflects better sampling of the diverse peat-forming environments in the transition from upper tidal marsh to freshwater environments.

Table 1: Summary statistics for transfer function models used to reconstruct paleo marsh surface elevations. All models use modern samples from the regional-scale dataset covering sites across south-central Alaska (Shennan et al., 2014b).

	Model 1		Model 2		Model 3	
	Previous version	New	Previous version	New	Previous version	New
Number of samples in modern training set	100	113	206	260	255	310
Number of components in weighted averaging partial least squares model[1]	2	2	2	2	2	2
Squared correlation between bootstrap predicted and observed values (r^2)	0.75	0.62	0.68	0.66	0.76	0.76
Root mean squared error of prediction (bootstrap RMSEP)	6.31	8.55	11.27	11.93	17.48	16.31
Improvement in RMSEP over one-component model	14.70%	5.41%	11.40%	8.71%	10.50%	10.41%
RMSEP scaled to tidal range at Girdwood (m)	0.21	0.29	0.38	0.40	0.59	0.55
RMSEP scaled to tidal range at Kasilof (m)	0.18	0.25	0.33	0.35	0.51	0.48
RMSEP scaled to tidal range at Beluga Slough (m)	0.16	0.21	0.28	0.29	0.43	0.40
Lithology of fossil sample to which the model can be applied	Peat		Silt / clay with herbaceous rootlets OR peat		Any, including silt, no visible rootlets or laminated clay, silt & fine sand	

[1] We assess model performance using boot-strapped r^2, scatterplots of observed and predicted values, and RMSEP, with the best models being those with the highest r^2 value, a linear distribution of observed plotted against predicted values, and the lowest RMSEP, but only if the RMSEP was improved by at least 5% with the addition of an extra component.

We have always argued that model performance and their subsequent elevation predictions are judged not only by the size of the error term but also by an assessment of the goodness of fit between each fossil sample and the modern dataset (Hamilton and Shennan, 2005a), as outlined above. When we apply the new transfer function models to all of our fossil data collected across south-central Alaska, i.e. those from our previous studies and the new sites in this report, we see an increase in the number of good modern analogues and consider this an important step in improving our confidence in the reconstructions of elevation change. We therefore accept larger error terms in order to have more good and close modern analogues.

Table 2: Comparison of goodness of fit between 1258 fossil samples with the new and previous modern datasets. Goodness of fit measured by the minimum chord distance dissimilarity coefficient between the fossil sample and the modern dataset. The 20th percentile of the dissimilarity values for the modern samples marks the cut-off between 'close' and 'poor' modern analogues for fossil samples, and the 5th percentile the threshold for defining 'good' modern analogues.

	new		previous	
	n	%	n	%
Good	305	24%	239	19%
Close	610	48%	606	48%
Poor	343	27%	413	33%
Total	1258		1258	

2.1.2 Conventions used for presentation of diatom data

In all of the diatom diagrams we show only those species >10% of the assemblage.

We classify each species according to their mean elevation (defined by the bootstrap species coefficient from the transfer function model) in the modern data set, dark blue = ~tidal flat elevations; mid blue = tidal marsh; light blue = upper marsh to freshwater; black cross-hatch = insufficient abundance of species sent in modern data set. This classification scheme is an aid to summarise the assemblage changes but does not take into account the elevation range of each species, only the mean. In contrast, the transfer function model reconstructions do account for these ranges.

The right-hand graph shows the changes in relative sea level (RSL), with 95% confidence limits.

For clarity, we do not show the goodness of fit between each fossil sample and the modern data on the diagram but we highlight in the text only where a change of RSL under discussion is based on samples with a poor modern analogue.

2.1.3 Radiocarbon results for both sites, Homer and Kasilof

We collected 21 samples for radiocarbon dating, using AMS methods on macrofossil samples picked from the sediment. We report the results in Table 3, along with two previously reported from Kasilof, with CAMS laboratory codes (Hamilton, 2003; Shennan and Hamilton, 2006), before discussing them separately in sections 3.1.4 and 3.1.5, and then collectively in sections 3.3 and 3.4.

Table 3: Radiocarbon ages

Code	Site #	Depth (cm)	Stratigraphic context	Material dated	14C age	1 σ	Calibrated age range (BP)			Median age (BP)
Homer: Beluga Slough										
OS-112093	BS-4	171.5	Peat B - top contact	Stem and probable root material	1230	20	1257	to	1072	1174
OS-112094	BS-4	382.5	Peat C - top contact	Small twig	2680	25	2844	to	2751	2778
OS-112095	BS-4	413	Peat C - base	Woody stem fragments	2880	20	3072	to	2945	3003
OS-112096	BS-4	424	Peat D - top contact	Small intact leaves	2740	25	2915	to	2772	2825
OS-112097	BS-4	453	Peat E - Top contact	Triglochin stem bases	3540	20	3891	to	3724	3837
OS-112098	BS-4	461	Peat E - base	Triglochin stem bases	3830	20	4346	to	4151	4214
OS-109768	BS-5	169.5	Peat B - top contact	Stem fragments and 1 seed	1120	20	1062	to	970	1018
OS-109769	BS-5	372.5	Peat C - top contact	Stem fragments and 9 seeds	2130	20	2293	to	2011	2116
OS-109770	BS-5	389	Peat C - base	Stem fragments	2250	20	2339	to	2159	2229
OS-109771	BS-5	406	Peat D - top contact	2 stem fragments	2550	20	2748	to	2519	2726
OS-109772	BS-5	441.5	Peat E - top contact	1cm long wood fragment	3390	25	3693	to	3576	3633
OS-109773	BS-5	452.5	Peat E - base	Grass and stem fragments	3670	25	4086	to	3920	4007
Kasilof										
OS-110179	KS-1	45.5	Peat 1 - top	Stem and leaf fragments	150	20	282	to	3	180
OS-110178	KS-1	55	Peat 1 - base	Stem and leaf fragments	925	30	924	to	769	852
OS-110177	KS-1	99	Silt - 1 cm above peat 2	Leaf fragments	1120	25	1166	to	960	1019
OS-110175	KS-1	100	Peat 2 - top contact	Single round stem	1050	20	1041	to	927	952
OS-110176	KS-1	100.5	Peat 2 - 1cm below contact	Stem and leaf fragments; Sphagnum	1240	20	1263	to	1082	1211
OS-110042	KS-1	104	Peat 2 - base	Stem and leaf fragments	1270	20	1270	to	1180	1229
OS-110041	KS-1	112	Peat 3 - top contact	Stem	1540	20	1522	to	1376	1462
OS-110040	KS-1	112.5	Peat 3 - 1cm below contact	Seeds, stem and leaf fragments	1630	25	1602	to	1416	1535
OS-110039	KS-1	190	Peat 3 - base	Stem and leaf fragments	5430	30	6290	to	6192	6240
CAMS-93965	KS-8	95	Peat 2 - top contact	Stem and leaf fragments	1150	30	1174	to	979	1061
CAMS-93966	KS-8	109	Peat 3 - top contact	Stem and leaf fragments	1570	35	1540	to	1386	1467

2.1.4 South shore of Kachemak Bay

Ghost forests, trees killed following submergence in 1964, occur at numerous locations on the south shore of Kachemak Bay. Based on satellite imagery and ongoing work, unpublished, by the Biological Monitoring Program of the Kachemak Bay Research Reserve, we targeted sites potentially least affected by local input of minerogenic sediment from the retreat of Little Ice Age glaciers.

Peterson Bay lies to the east of a rocky peninsula that separates it from China Poot Bay. The catchment of the latter receives significant modern minerogenic sediment from Wosnesenski Glacier and Doroshin Glacier. We found much of the ghost forest directly rooted within coarse gravel. Finer minerogenic sediments occur in one sheltered part of western Peterson Bay where a small ghost forest extends landward into a peaty swamp. Coring across this swamp revealed only a few decimeters of organic sediment over gravel, boulders or rock and no evidence of repeated submergence.

Sadie Cove is a 9 km long fjord, with no glacier presently in the catchment. There is a marsh and small ghost forest at the head of the cove and it forms part of the Biological Monitoring Program of the Kachemak Bay Research Reserve, http://www.adfg.alaska.gov/index.cfm?adfg=kbrr_research.home. We completed more than 20 trial cores across the marsh and found all ended on impenetrable gravel within 1m. The deepest sequences revealed no sediment sequences with unambiguous paleoseismic evidence other than the small ghost forest.

Because of these findings at Peterson Bay and Sadie Cove, we decided to concentrate resources on the sites at Beluga Slough, Beluga Wetlands and Kasilof.

2.1.5 Homer: Beluga Slough and Beluga Wetlands

The road from Homer Township to Homer Spit runs along an embankment that separates Beluga Lake from Beluga Slough. A sluice gate controls the water level of the lake for the operation of the floatplane facility. Prior to the construction of this embankment in the 1950s, intertidal marshes and sand/mud extended eastwards to the head of the lake. The freshwater marsh merges into raised bog that extends east with peat sequences exposed on the shore around Miller's Landing (Figure 2b). At this location, Waythomas (2000) describes a 4 to 6 m high bluff with a sequence, from the base upwards, of fibrous peat, silt-peat, and slightly organic, thin-bedded-to-massive clay-silt, interpreted as a tidal flat deposit, and then a surface peat. The entire sequence lacked evidence for unconformities or marine sediments that could be interested as tsunami deposits. A wood sample from the base yielded a radiocarbon age of 2805±95yr BP (GX-21322). The contact to the tide-flat was gradational and a wood sample in the top of the peat gave a date of 1460±20 yr BP (GX-21369). Begét et al. (2008) also describe a section of the bluff at Miller's Landing, recording a peat sequence that started forming around 8000 years ago, with no equivalent unit to the tide-flat clay-silt unit. They interpreted two sand layers within the freshwater peat unit as tsunami sediments, with one radiocarbon dated 3570 ± 70 yr BP and 3760 ± 70 yr BP (no codes reported) and recorded ~0.9 m above the present high tide line.

Waythomas (2000) also describes the results of cores from Beluga Slough marsh, noting that a peat sample from about 4.5 m depth in one of the cores yielded a radiocarbon age of 3100±80 yr BP (no code reported).

At Beluga Slough, a sand and gravel spit dampens the tidal range between the spit and the road embankment (Figure 2b), with mechanical removal of sediment intermittently required to keep the channel open. The Slough was as an anchorage for Homer in the early 20th century, with dredging required to keep it accessible.

We conducted two sets of sampling, in Beluga Wetlands and Beluga Slough, separated by the Beluga Lake, which was inaccessible due to the floatplane operations. Along the central axis of Beluga Wetlands we recorded thick, >5.5 m, freshwater peat that we could not bottom out (BW1 and 2 in figure 2c). Near to the base, we found two thin silt/sand layers that we interpret as tephra. We could not extend the sampling closer to Beluga Lake due to waterlogging and the surface peat floating on water. Access to this part of the wetland would require a boat and access arrangements with the airport and float plane facility. Other cores, to the side of the wetland close to the bluff that the airport stands on show intercalations of organic, limnic and minerogenic sediments, with no sequence of units that we could trace easily between cores. We interpret the coarse minerogenic sediments as slope wash from the bluff.

Hand drilled cores demonstrated more than 6 m of unconsolidated sediments in Beluga Slough, with the deepest cores, BS3 and BS5 (Figure 2c) ending within a silt unit rather than stopped by rock or gravel. Most of the cores reveal multiple peat-silt alternations, usually with a sharp upper contact of the peat, and quite often with a sharp lower contact too. Figure 3 illustrates one example. We find it difficult to correlate these thin, multiple couplets between boreholes. In figure 2c we show our best interpretation of the field data, suggesting 5 contacts that we feel we have some confidence in their continuity, based on the lithology of the organic and minerogenic layers than form the couplet and their stratigraphic position with respect to layers above and below. We label these down core as Contact A to Contact E.

Cores 1 and 2 are adjacent to exposures alongside the present channel of Beluga Slough. We could not sample the exposures directly as they were mostly below water level even at low tide but we observed numerous examples of sawn timber at the upper contact of the peat with the overlying silt unit. We infer this contact most likely to be AD 1964, where the reported coseismic submergence is approx. 0.9 m (Plafker, 1969); alternatively, it may reflect a rapid change in the tidal dynamics of the intertidal system resulting from construction of the causeway to create Beluga Lake in the 1950s.

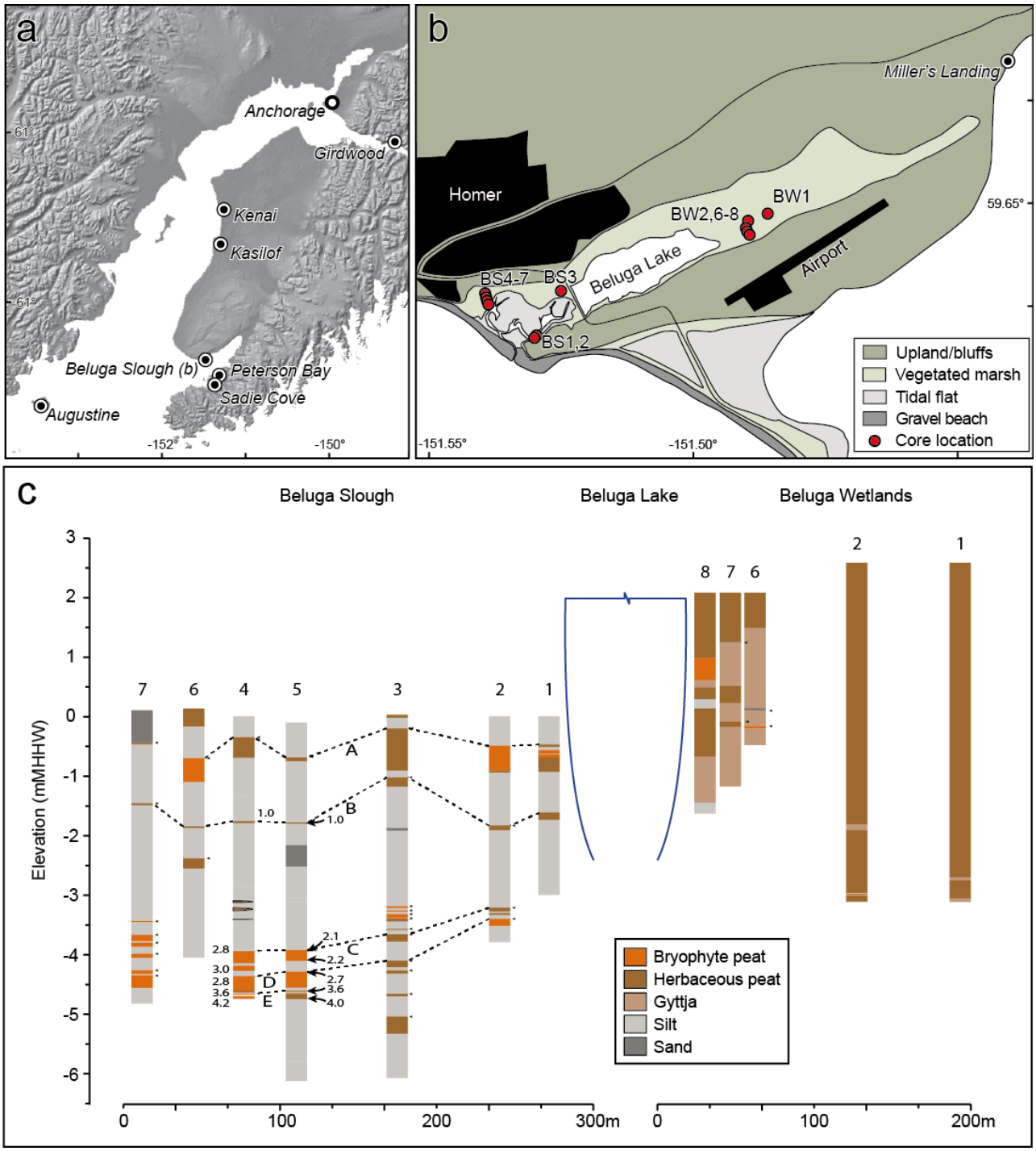

Figure 2: a) site locations; b) Homer core locations at Beluga Slough and Beluga Wetlands; c) stratigraphy of cores, with suggested correlations of peat-silt contacts A through E and radiocarbon ages, summarised by median age ka BP with full details in Table 3.

Figure 3: Core BS3 298-364 cm – example of multiple thin peat and silt layers

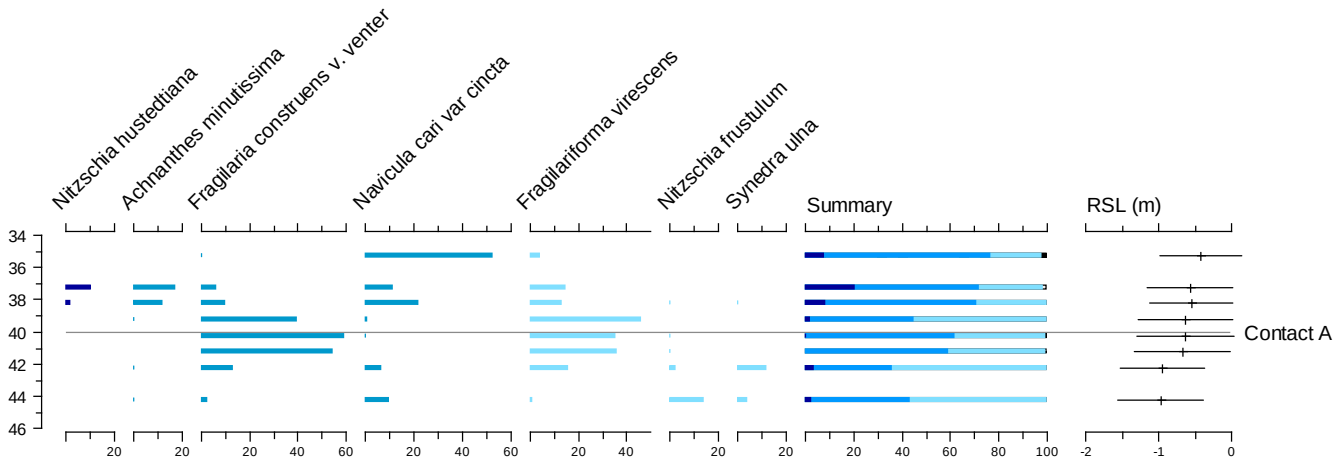

Figure 4: Beluga Slough contact A, core 4, diatom diagram showing individual species >10% in at least one sample and summary classes, %, of all species counted; summary classes based on species optimal elevations in the modern data set, dark blue = ~tidal flat elevations; mid blue = tidal marsh; light blue = upper marsh to freshwater; black cross-hatch = insufficient abundance of species sent in modern data set. Right-hand graph shows the changes in relative sea level (RSL), with 95% confidence limits, estimate by the transfer function model. Vertical axis is depth, cm.

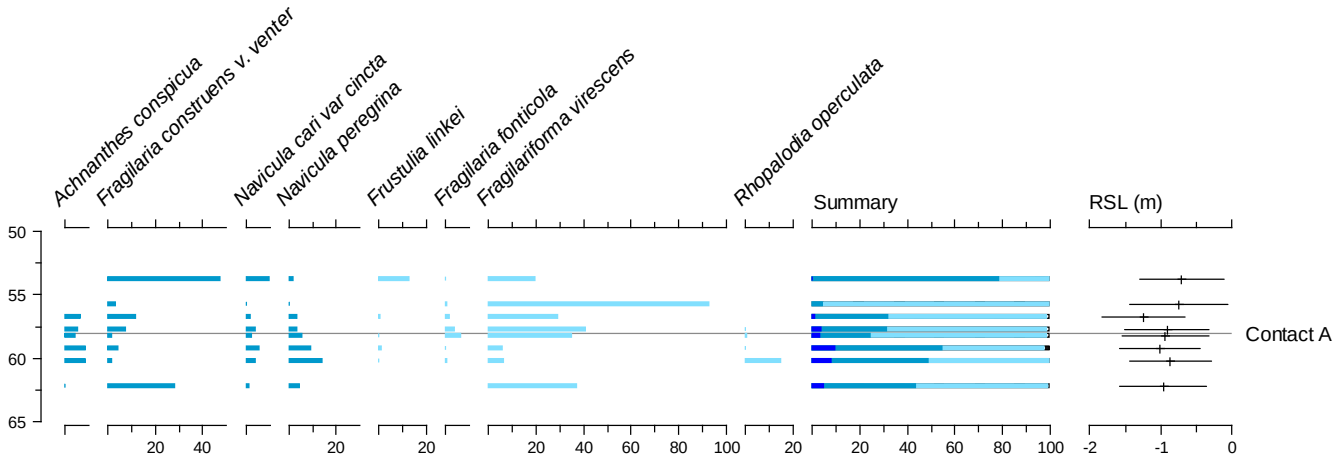

Figure 5: Beluga Slough contact A, core 5, other details as Figure 4.

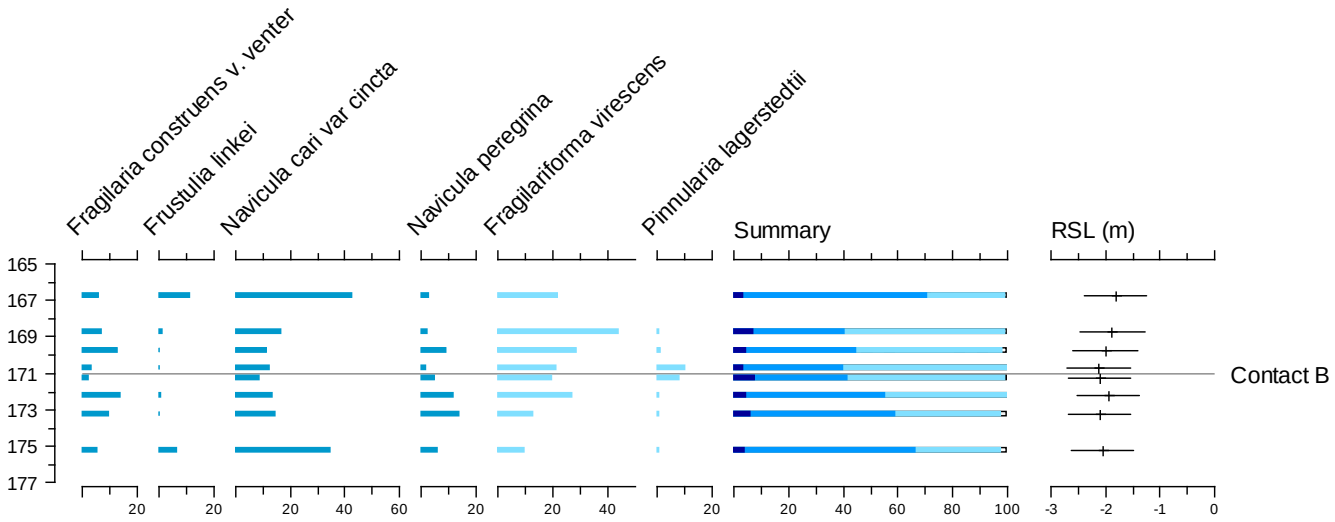

Figure 6: Beluga Slough contact B, core 4, other details as Figure 4.

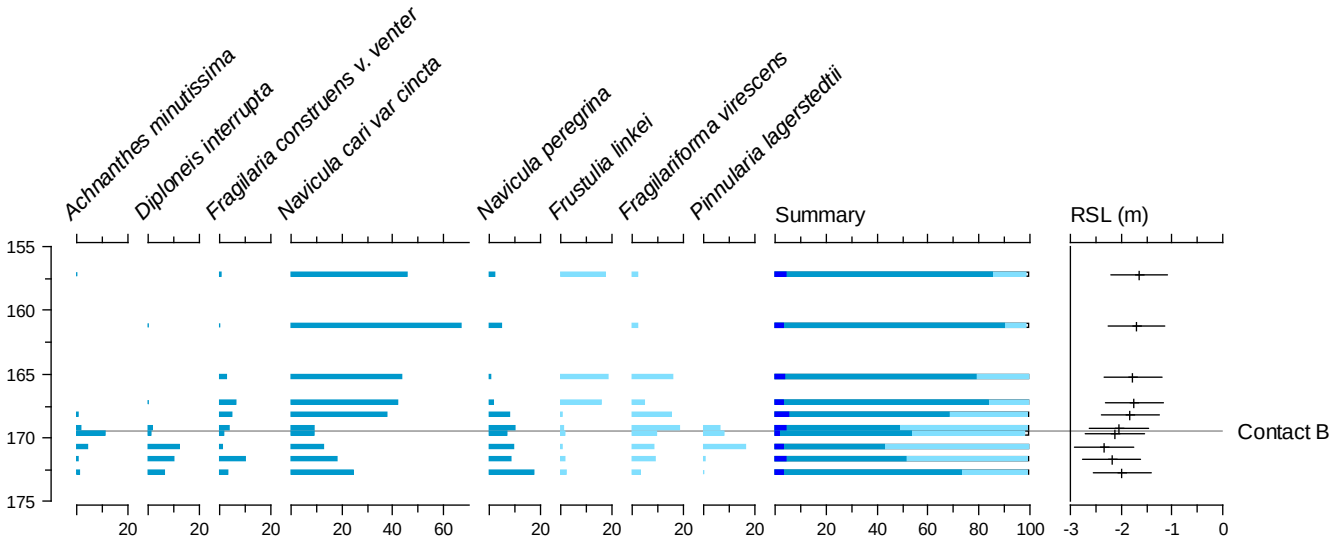

Figure 7: Beluga Slough contact B, core 5, other details as Figure 4.

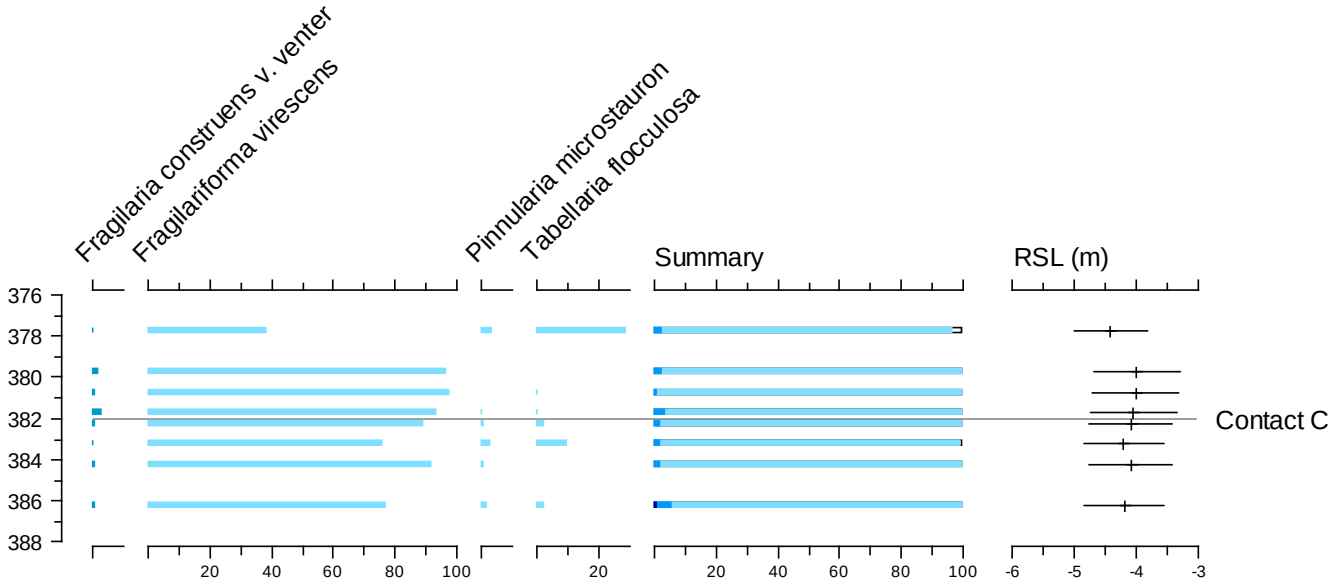

Figure 8: Beluga Slough contact C, core 4, other details as Figure 4.

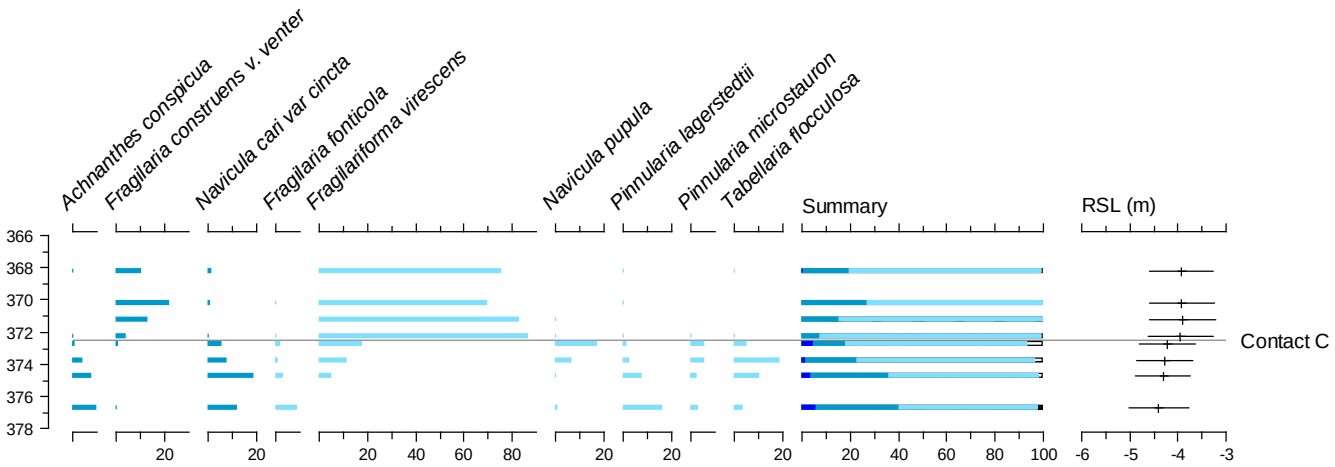

Figure 9: Beluga Slough contact C, core 5, other details as Figure 4.

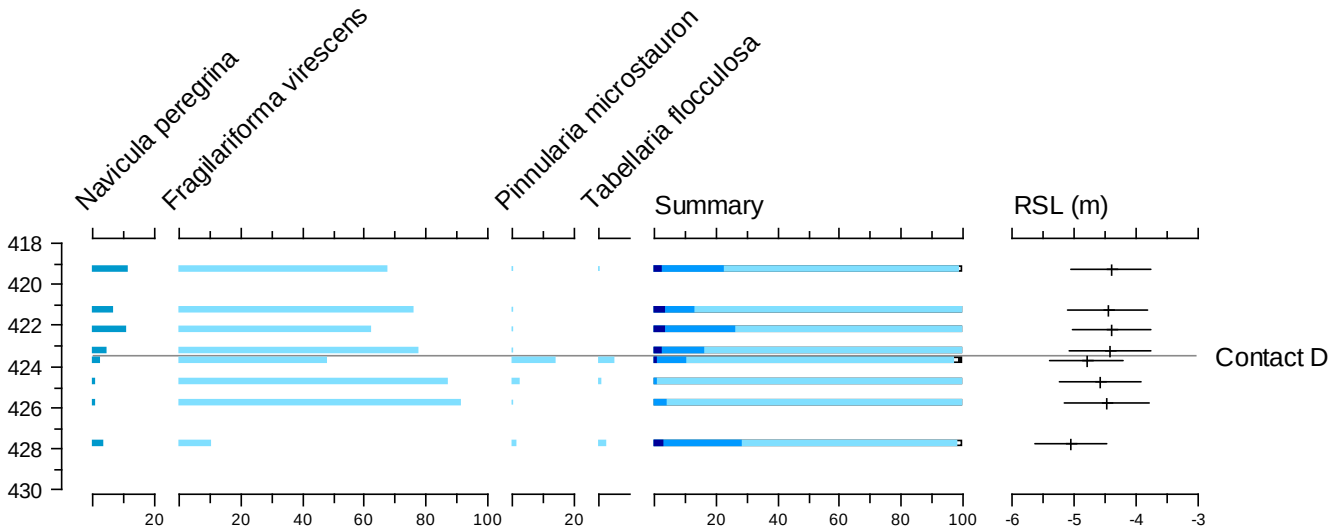

Figure 10: Beluga Slough contact D, location 5, other details as Figure 4.

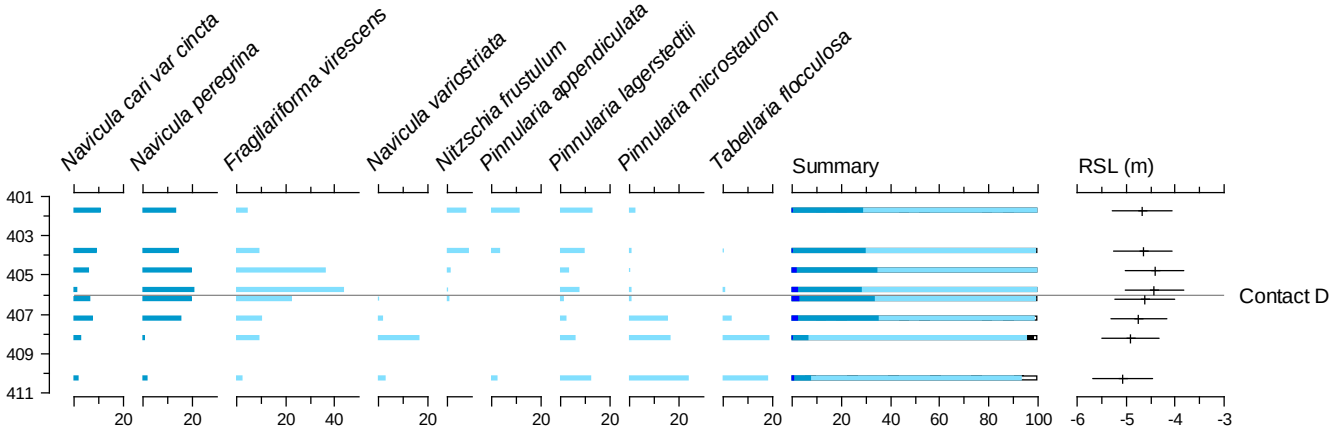

Figure 11: Beluga Slough contact D, core 5, other details as Figure 4.

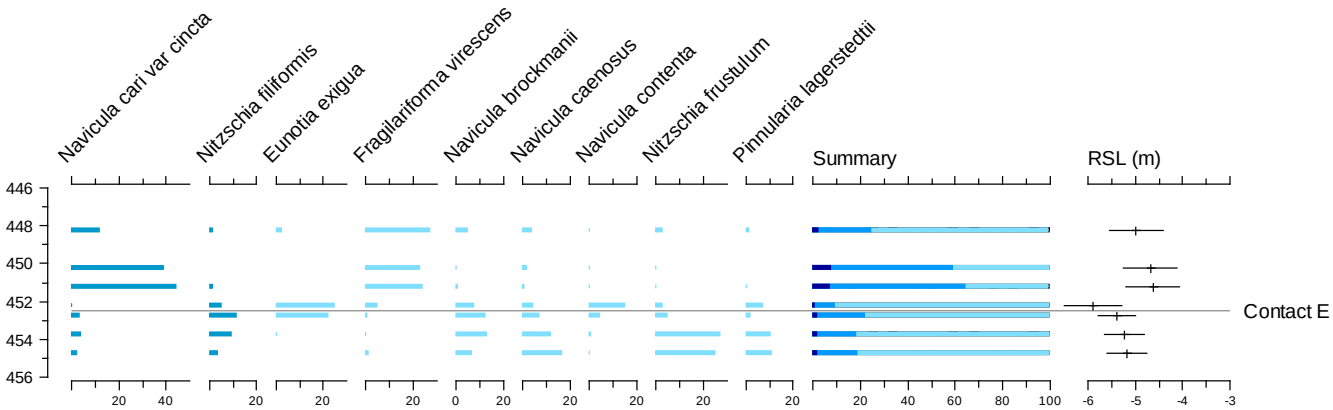

Figure 12: Beluga Slough contact E, core 4, other details as Figure 4.

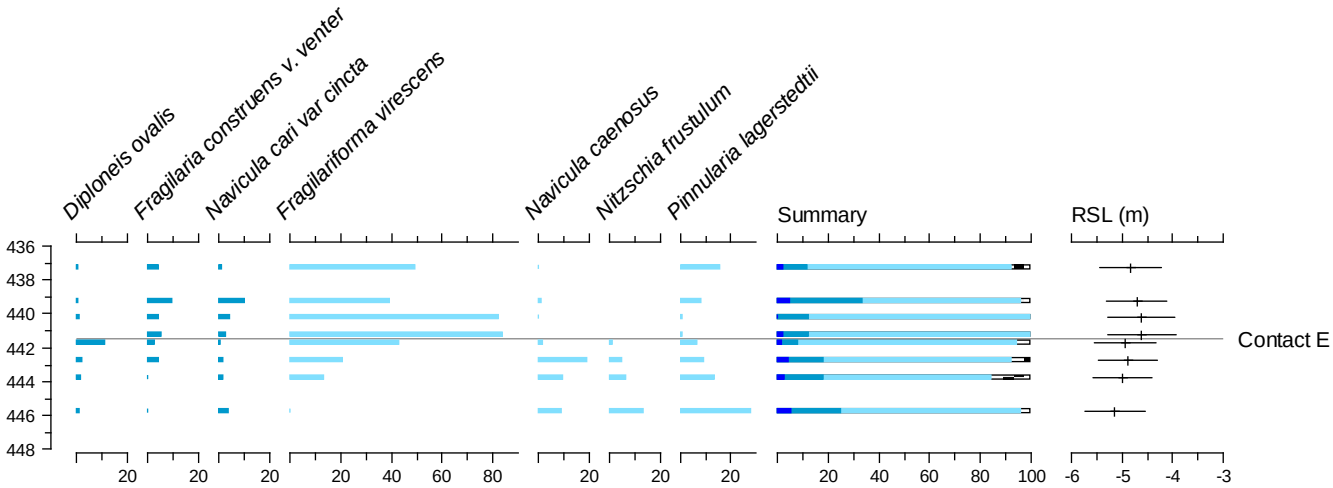

Figure 13 Beluga Slough contact E, core 5, other details as Figure 4.

Most of the diatom analyses share common characteristics: dominant species that reflect freshwater environments, e.g. *Fragilariformis virescens*, or the transition from highest tidal environments to freshwater systems where we get a mix of freshwater species, e.g. *Fagilaria construens* var *venter, Pinnularia lagerstedtii* and brackish-water species, e.g. *Navicula peregrine, Navicula cari* var *cincta*.

In both core 4 and core 5, contact A shows very little change in diatom assemblages that would suggest rapid relative sea-level rise due to coseismic subsidence if this is the 1964 horizon and also the transfer function reconstructions indicate a gradual rise in RSL rather than the 0.9 m observed in 1964.

Contact B is very similar to contact A, gradual changes in fresh and brackish water species and no clear, rapid rise of sea level across the contact.

Contact C shows differences between the two cores, so may suggest the correlation is incorrect or may suggest that only the location closer to the centre of the embayment was sensitive to the small change in environment al conditions. The radiocarbon ages (Table 3) for contact C and D indicate likely sediment reworking.

Contact D shows changes at both cores, reversing some of the trends in place below the contact in each core and a small RSL rise across the contact, followed by stable or falling RSL.

Contact E does show some rapid changes across the contact, and both cores could record a small rise in RSL, median estimate in the order of <0.5 m.

In order to test the hypothesis of coseismic submergence being recorded we compare the evidence for each contacts against the Nelson et al. (1996) criteria: lateral extent of peat-mud couplets with sharp upper contacts; suddenness of subsidence; amount of subsidence; synchroneity of subsidence with other sites; and presence of tsunami deposits at the contact). Figure 14 compares the ages the contacts of the contacts with those for great earthquakes recorded across the Prince William Sound segment (Shennan et al., 2014c).

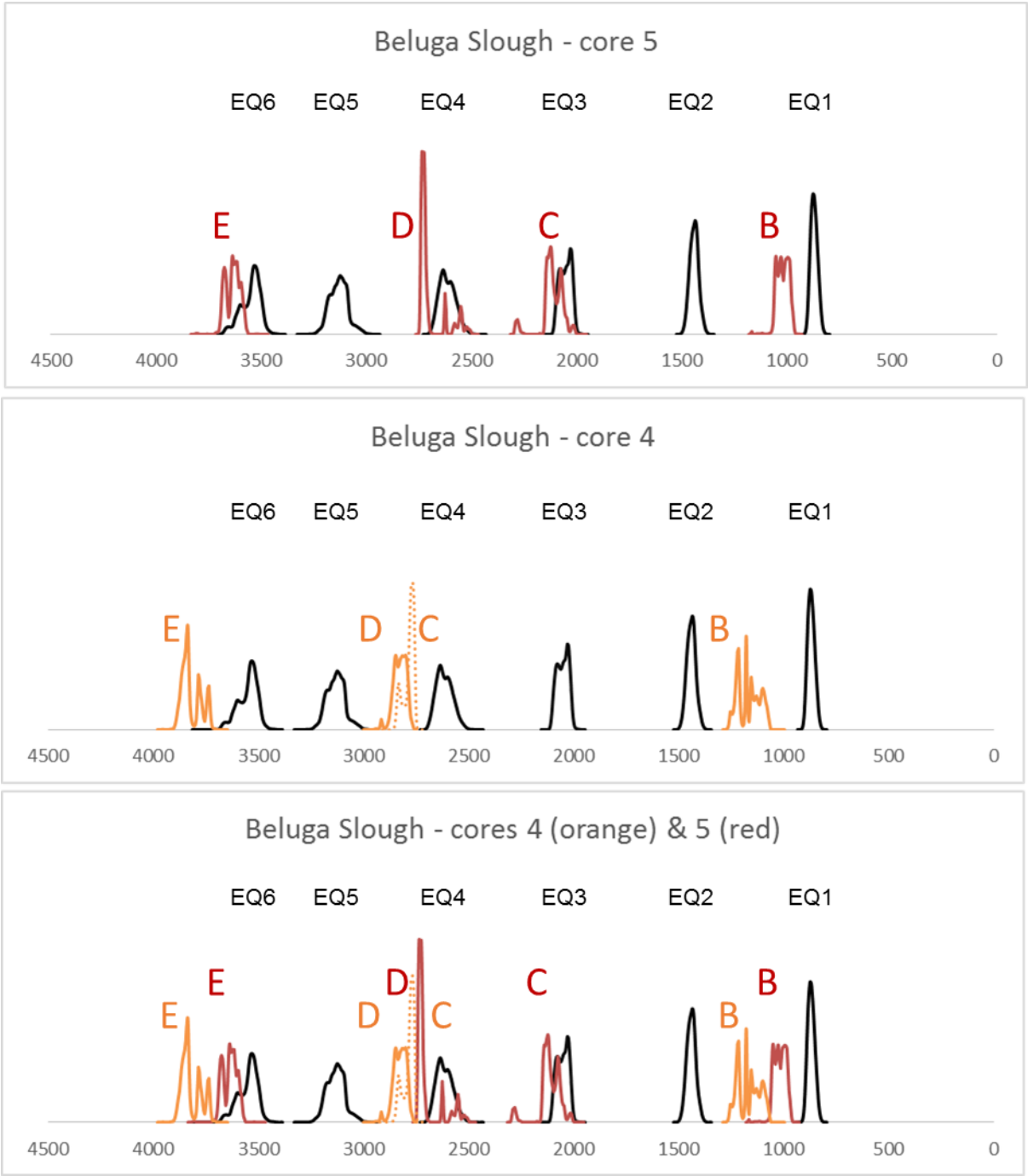

Figure 14: probability density functions of the radiocarbon ages for contact B to E (details in Table 3) compared to those for six, pre 1964 great earthquakes recorded across the Prince William Sound segment, labelled EQ1 through 6 (Shennan et al., 2014c).

The evidence for synchroneity with the Prince William Sound segment differs between the two cores. Core 5 shows a good correlation for three of the four contacts, but core 6 shows no close correlation unless we consider that there has been erosion of the peat at each contact. This is always possible as the ages are maximum ages for any episode of rapid submergence

	A	B	C	D	E
Lateral extent	good	good	Ok/poor	ok	limited
Suddenness	poor	poor	In core 5	poor	mixed
Amount (mean estimate)	none	~0	<0.5 m	<0.5 m	<0.5 m
Synchroneity	N/A	poor	possible	equivocal	equivocal
Tsunami deposit	no	no	no	no	no

Table 4: summary of the evidence from cores 4 and 5 for each contact assessed against the criteria of Nelson et al. (1996) for identifying a likely coseismic cause.

We conclude that the abrupt changes in stratigraphy the cores from Beluga Slough do not fulfil the criteria to support strongly the interpretation of coseismic subsidence as the probable cause. We suggest that non-seismic, dynamic changes in the barrier across the mouth of Beluga Slough offer an alternative explanation for the abrupt changes in lithology and diatom biostratigraphy. The diatom assemblages show that both the minerogenic and peat layers indicate sedimentation above MHHW with no large changes in sea level across stratigraphic contacts. The present tidal regime shows low water behind the barrier just below MHHW level in the open waters of Cook Inlet (Figure 15). The elevation of low water and ponding behind the barrier will vary according to the dynamics of the barrier, as will the supply of sediment into the tidal system.

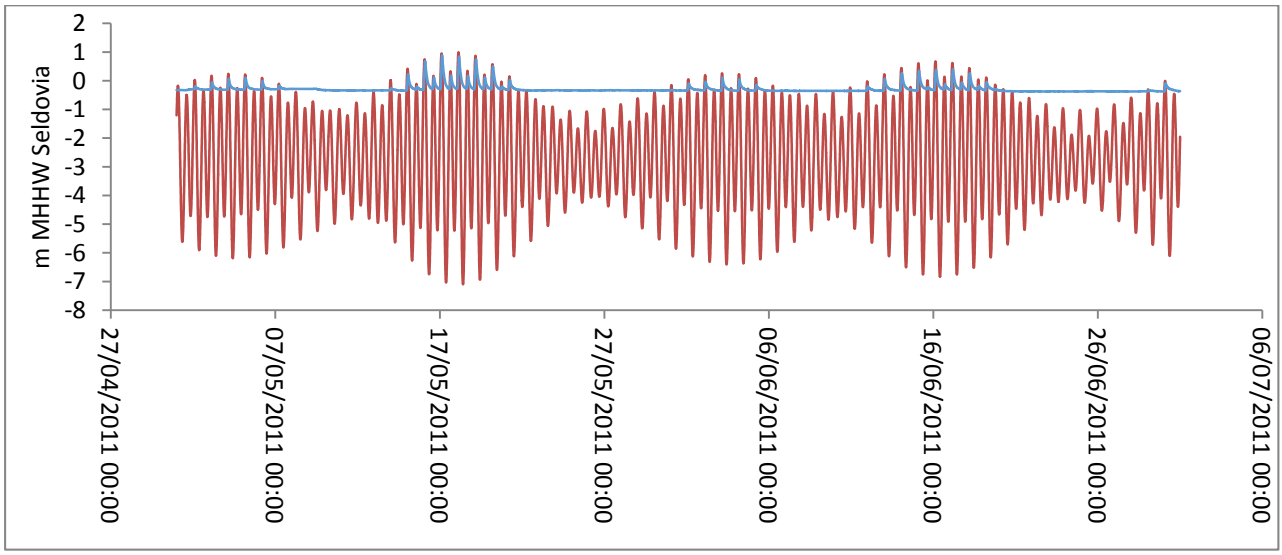

Figure 15: Water levels at NOAA tide station at Seldovia (red) and waterlogger installed in Beluga Slough (blue), by Steve Baird, Kachemak Research Reserve, Homer.

In terms of paleoseismological evidence for marsh submergence we cannot exclude the possibility that great earthquakes can trigger a change in the morphology of the barrier and sedimentation in the marsh behind. Similar changes occurred in comparable environments across south central Alaska in 1964 (Plafker, 1969). The coincidence of ages for at least three contacts in core 5 (Figure 14) suggest there could be a coseismic signal, but the RSL change is less than in 1964.

In terms of seismic hazard, we also conclude that there is no evidence for submergence greater than 1964 and no evidence for tsunami deposits. The latter conclusion agrees with the findings of Waythomas (2000) rather than Begét et al. (2008).

2.1.6 Kasilof

Previous reports describe peat-mud couplets at Kasilof, but their radiocarbon dating control is based only on bulk radiocarbon samples with the age of a bulk peat sample at the base of the approximately 6300 cal. yr BP (Combellick and Reger, 1994). Erosion and slumping along the tidal channel of Kasilof River exposed an almost continuous section in 2013, very similar to those described previously and reveal that the peat-mud couplets extend > 200 m along the channel. We cleaned a number of sections before selecting one to sample that was free from slumping. We also made hand-drilled cores in a transect perpendicular to the channel in order to assess the lateral continuity of each couplet (Figures 16 and 17).

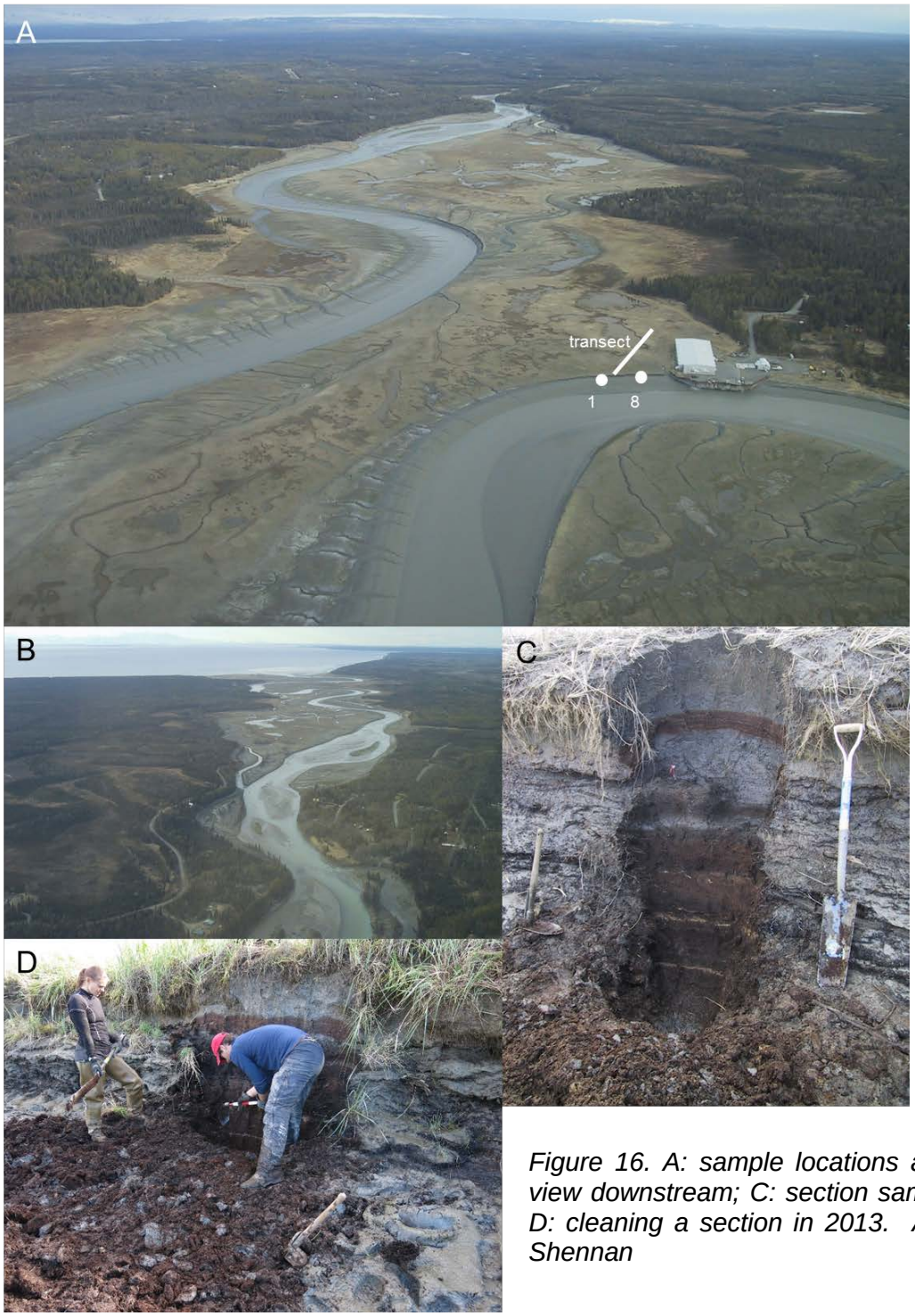

Figure 16. A: sample locations and view upstream; B: view downstream; C: section sampled 2001, location 8; D: cleaning a section in 2013. All photographs by Ian Shennan

Our results indicate three peat layers close to the present channel and two as the sequence gets thinner towards the bluff cut into the bluff of the Kalifornsky Glacioestuarine Terrace (Reger et al., 2007). Radiocarbon results give the age of peat 1 ~900 to 200 BP, median values, see Table 3 for ranges.

Preliminary Cs^{137} indicated AD 1964 occurs within the silt well above the upper contact of peat 1 (Hamilton, 2003). To check this finding we sampled at the top contact of peat 1 and found no detectable Cs^{137} so confirm that the upper contact of peat 1 is not AD1964.

Peat 2 formed within ~ 200 years, 1200 to 1000 BP, while peat 3 spans a much longer age range, ~ 6200 to 1500 BP.

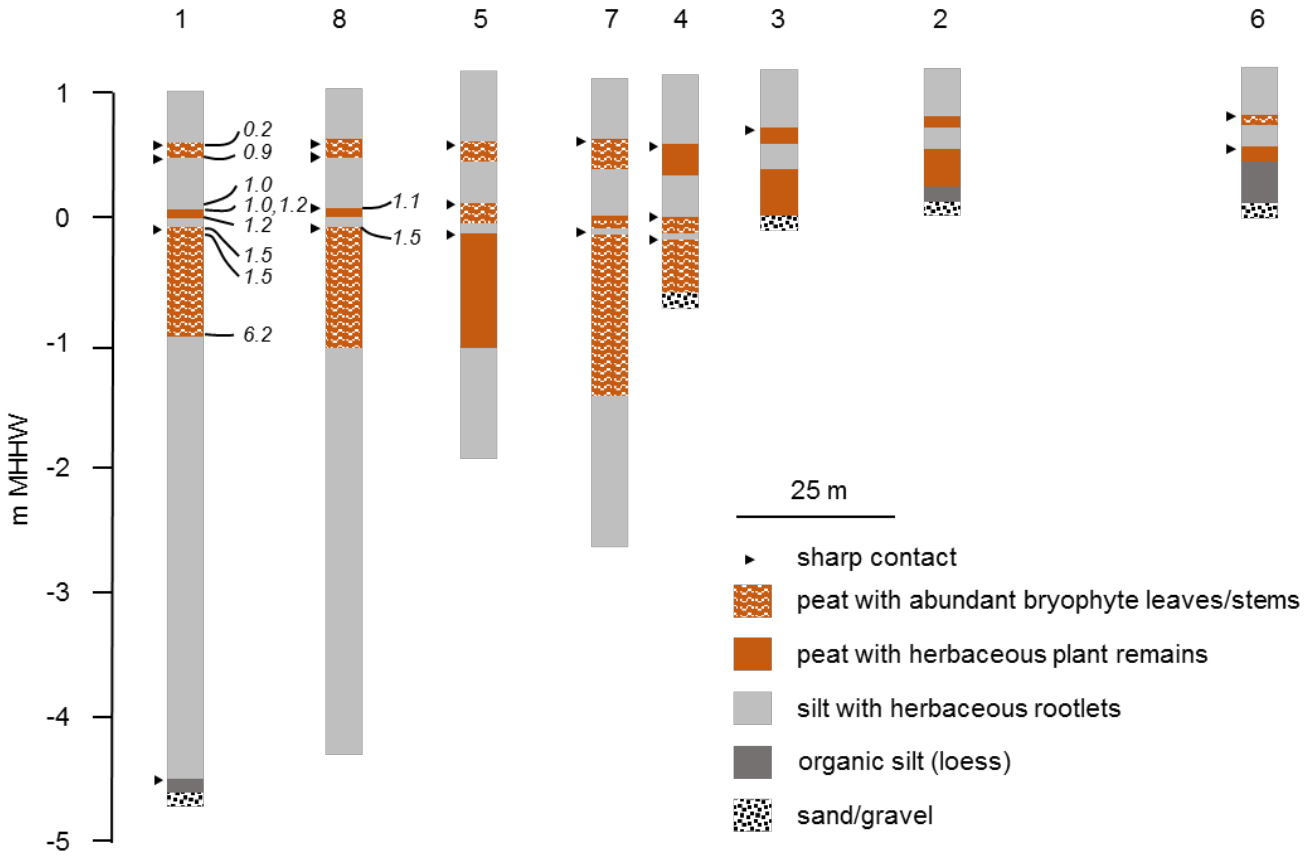

Figure 17. Kasilof cross section derived from exposures and coring. Calibrated radiocarbon ages summarised by median age, ka BP (full details in table 3). We see three distinct peat layers extending from location 1 to location 4 and refer them as peats 1, 2 and 3, numbered down section from the surface.

For diatom analyses we validated the original counts of Hamilton (2003), reclassified each species in line with the new transfer function model described in section 3.1.1, completed new diatom analyses across the key sediment boundaries (Figure 18) and performed transfer function reconstructions of elevation changes for all samples (Figure 19 to 23).

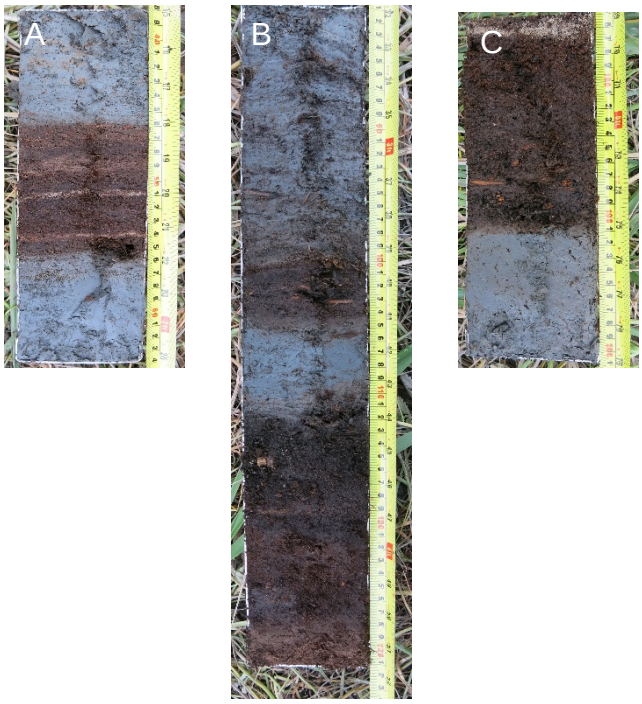

Figure 18: Box samples collected from site 1 for diatom and radiocarbon analyses; A, across peat 1; B, across peat 2 and top of peat 3; C, base of peat 3

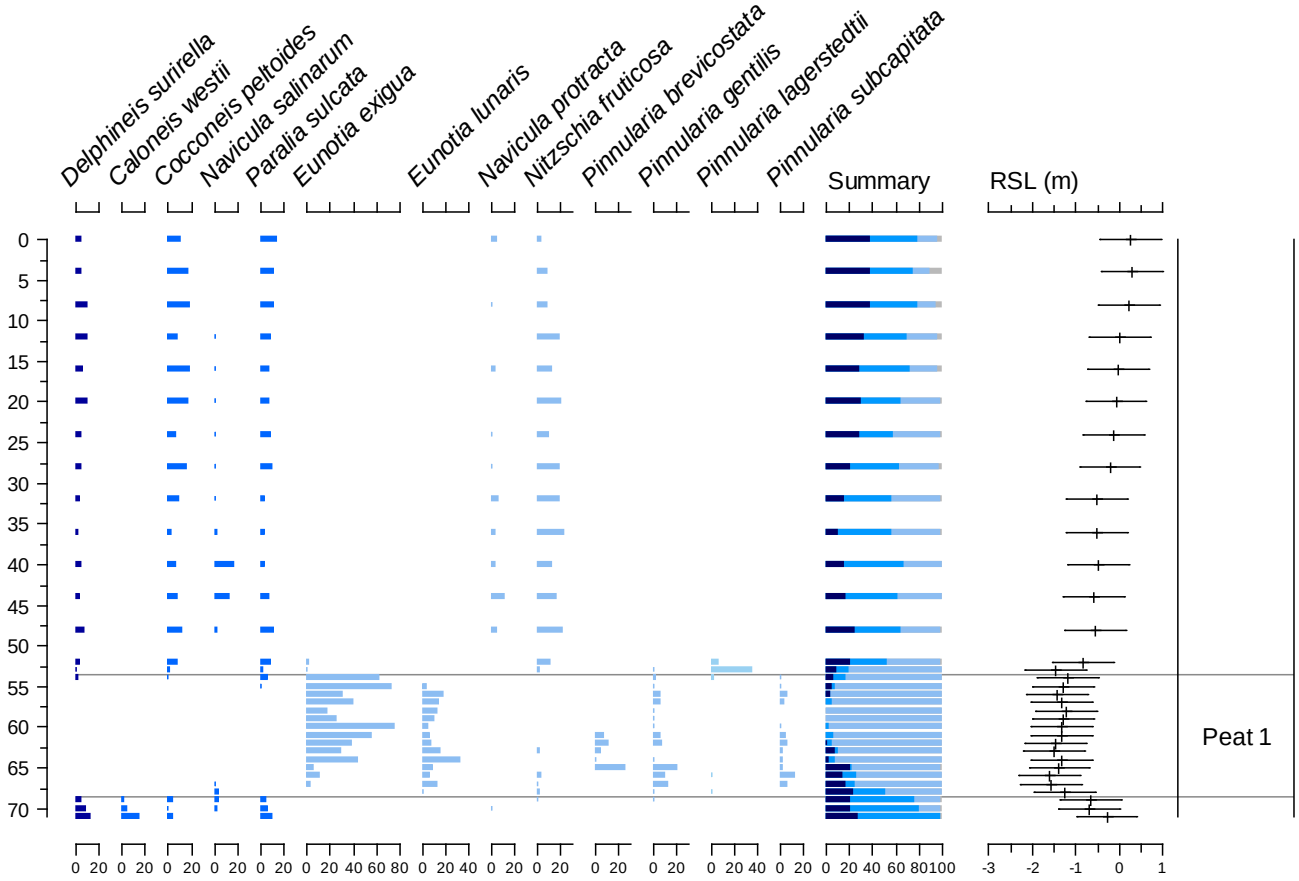

Figure 19: Kasilof 8, upper section, peat 1 to surface, diatom diagram. Graphs show individual species >10% in at least one sample and summary classes, %, of all species counted; summary classes based on species optimal elevations in the modern data set, dark blue = ~tidal flat elevations; mid blue = tidal marsh; light blue = upper marsh to freshwater; black cross-hatch = insufficient abundance of species sent in modern data set. Right-hand graph shows the changes in relative sea level (RSL), with 95% confidence limits, estimate by the transfer function model. Vertical axis is depth, cm. Original counts

(Hamilton, 2003) reclassified and analysed using the new modern training set and transfer function model described in section 3.1.1.

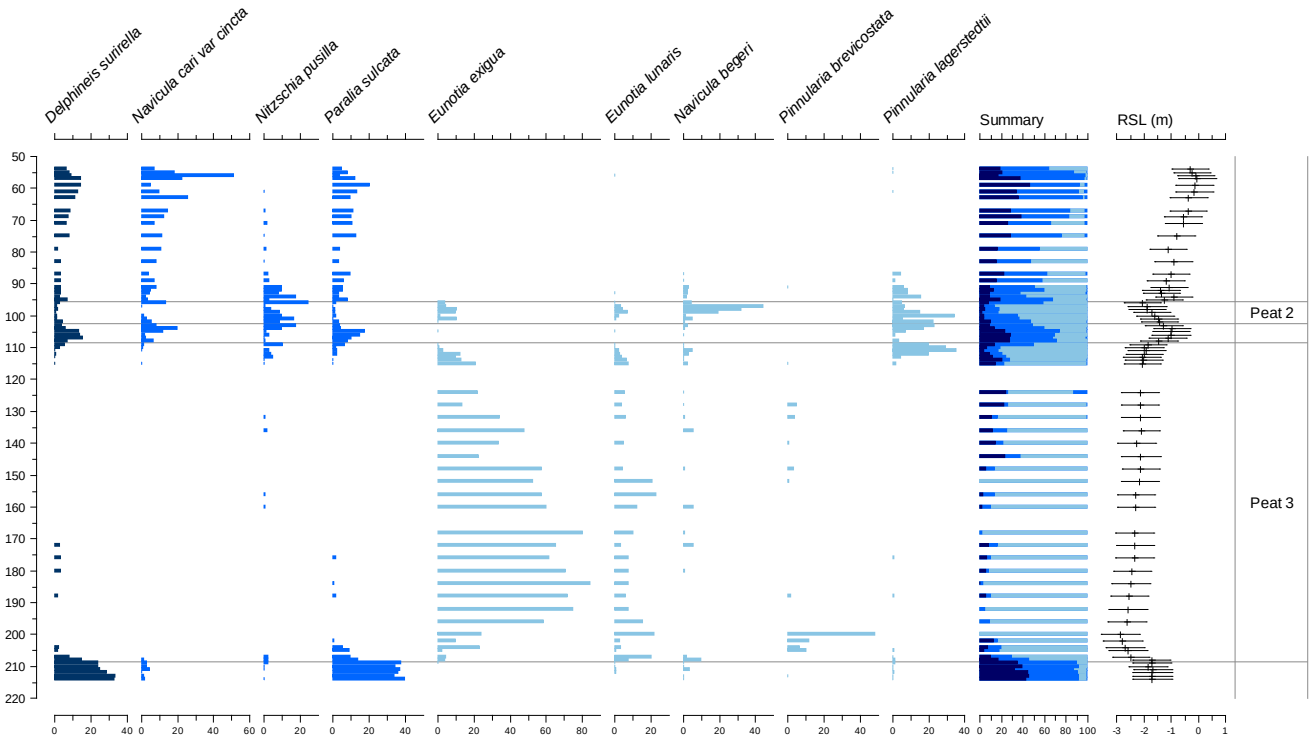

Figure 20: Kasilof 8, lower section, including peat 2 and 3, diatom diagram. Other details as figure 19. Original counts (Hamilton, 2003) reclassified and analysed using the new modern training set and transfer function model described in section 3.1.1.

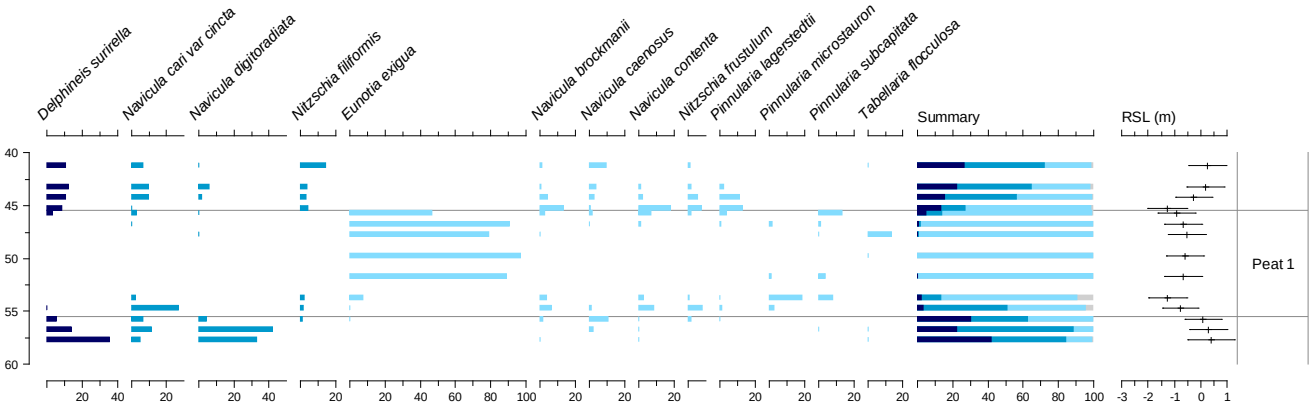

Figure 21: Kasilof 1, peat 1, diatom diagram. New diatom counts, other details as figure 19.

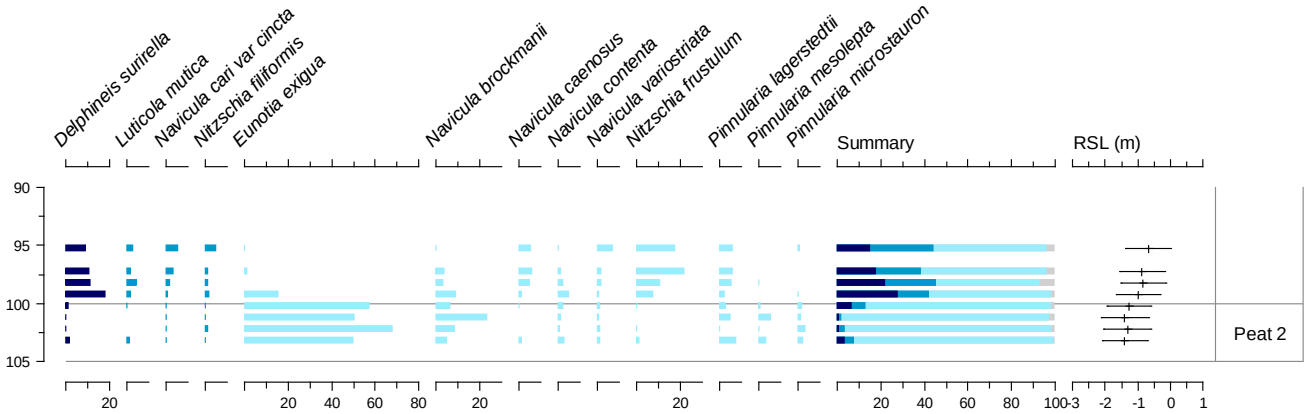

Figure 22: Kasilof 1, peat 2 upper contact, diatom diagram. New diatom counts, other details as figure 19.

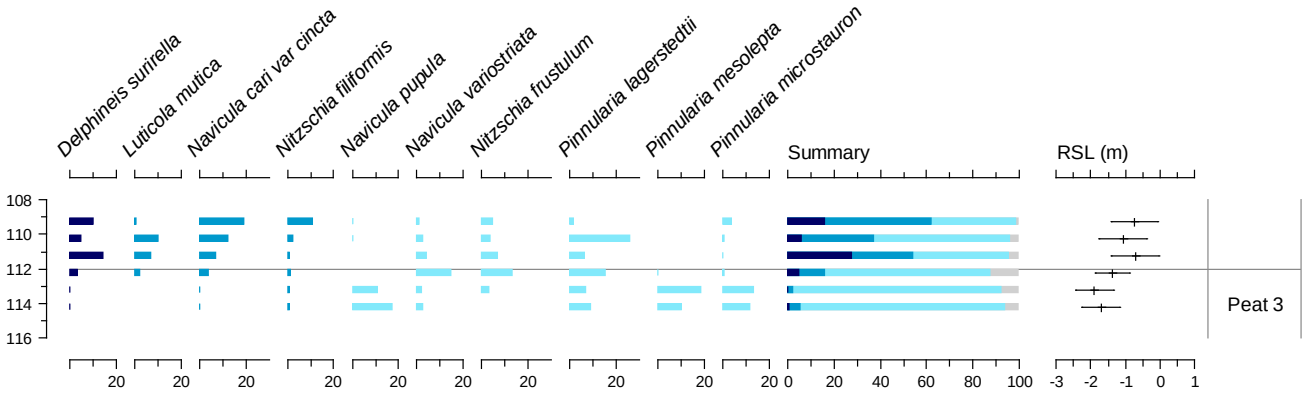

Figure 23: Kasilof 1, peat 3 upper contact, diatom diagram. New diatom counts, other details as figure 19.

The diatom data show that all of the clastic sediments indicate deposition in an intertidal environment. In peat 1 and peat 3, the assemblages are predominantly freshwater, whereas peat 2 has a mix of species reflecting tidal flat through to freshwater preferences. Changes across the top contact of each peat layer are quite abrupt and reflect a rapid change in environment. We shall consider each contact with reference to the Nelson et al. (1996) criteria for assessing seismic v. non-seismic causes of marsh submergence, in particular the potential impact of fluvial processes. The Kasilof River drains 1,919 km^2 of the Kenai Mountains and Kenai Peninsula lowlands and in addition to the potential of major floods from Tustumena Lake it also receives infrequent outburst flooding from lakes impounded by Tustmena Glacier (Reger et al., 2007). Imagery of the tidal section, ~8 km, (Figure 16A,B) shows a dynamic system with evidence of changes in meander patterns, undercutting of channel sides and packages of sediment deposited adjacent to the channel. Away from the channel, the marsh surface is relatively flat, with small changes in topography, <0.1 m, delimiting ponds of standing water from vegetated marsh. We envisage major floods, whether from snowmelt, rainfall or lake outbursts, may cause morphological changes that are recorded in the stratigraphy. These include a temporary pulse of minerogenic sedimentation, channel erosion and possible avulsion. We summarise our interpretation of the sediment and diatom stratigraphies below.

The change to a freshwater environment ~6.2 ka BP (Table 3; Figure 17) reflects the balance between relative sea-level change and sediment input, continuing the infilling of the estuarine system that was on going since at least 10 ka BP (Combellick and Reger, 1994). A pulse of sediment raising the intertidal flat may help explain the quite rapid transition seen in the sediment stratigraphy (Figure 18C) compared to the transition evident in the diatoms (Figure 19).

The contact at the top of peat 3 fulfils the criteria as evidence of cosesimic submergence. We can trace the contact laterally (Figure 17), the contact is abrupt (Figure 18B) and the diatoms show a rapid change, with subsidence in the order of 0.5 m (Figures 20 & 23). It is possible that local processes, including river flooding, could produce comparable sediments but further evidence supports the coseismic hypothesis. First, the age of the contact is synchronous with evidence of coseismic submergence at Kenai, just to the north and more widely across south central Alaska (Figure 24). Second, the gradual trend of RSL fall, from the base of the silt above peat 3, through the silt and through peat 2, fits with the model of century-scale interseismic uplift following coseismic subsidence (Shennan and Hamilton, 2006).

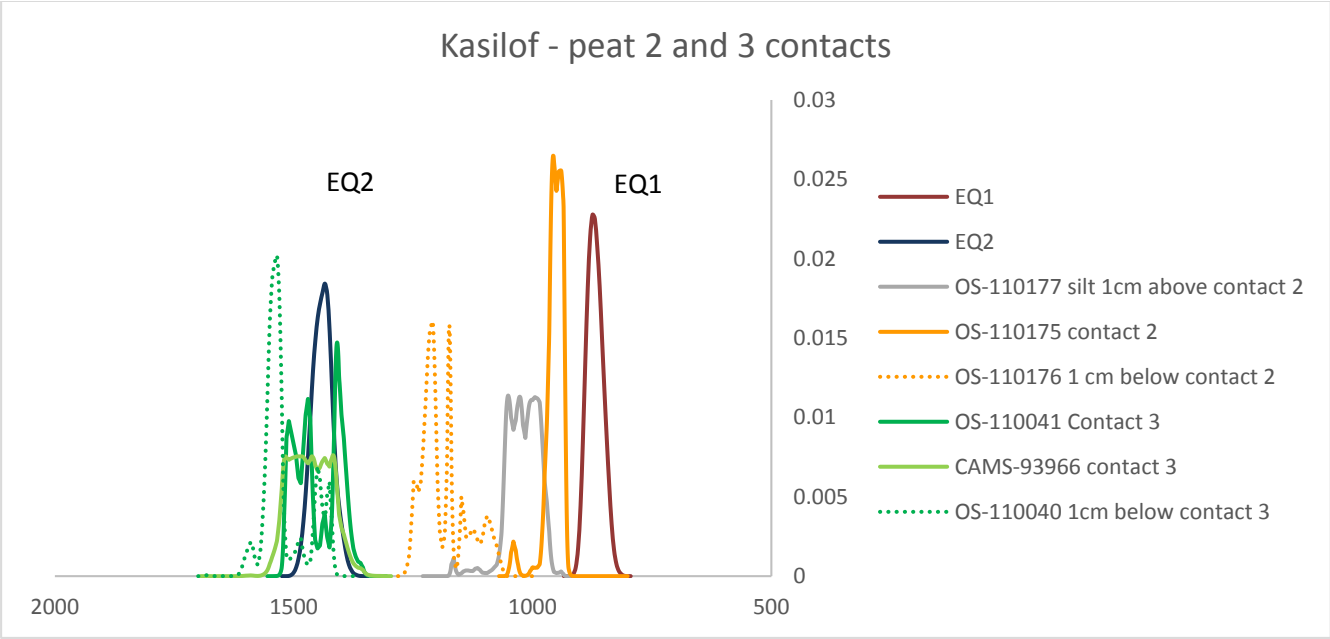

Figure 24: probability density functions of the radiocarbon ages for contacts 2 and 3 (details in Table 3) compared to those for pre 1964 great earthquakes recorded across the Prince William Sound segment within the last 2000 years (Shennan et al., 2014a).

The top of peat 2 records a rise in sea level but we do not consider it as evidence of coseismic subsidence for the following reasons. First, the boundary is sometimes sharp and sometimes diffuse (Figure 17 & 18B). Second, the diatoms show a rapid change in one reconstruction (Figure 20) and gradual in another (Figure 22); and third, the age is not synchronous with events recorded elsewhere (Figure 24), even the nearest site Kenai.

We also do not consider Peat 1 as recording cosesimic subsidence, even though it occurs across the transect (Figure 17), with a sharp upper contact in all except one core. The key lines of evidence are the diatom analyses from exposures at locations 1 and 8 (Figure 19 & 21). Both show a rapid change in diatom species between the sample from the top of the peat and that from the base of the silt, but the assemblage in the latter indicates sedimentation continuing in a mainly freshwater environment and no change in sea level. Sea-level rise occurs only gradually through the remainder of the silt horizon, to the present surface. We suggest that this is initially a river flood that inundates the peat environment, followed by gradual sea-level rise. The age of for the top contact is not synchronous with great earthquakes recorded elsewhere in the region (Figure 24).

2.2 Research Question 2. Is there evidence of Late Holocene earthquake-generated tsunami?

We find no evidence for tsunami deposits at Homer and Kasilof. As noted above, regarding Homer, this agrees with the findings of Waythomas (2000) rather than Begét et al. (2008).

2.3 Research Question 3. How do spatial patterns of estimated land-level changes for different Holocene plate boundary earthquakes vary between Kodiak Island and western Yakataga?

Our new findings add to the growing body of evidence that suggest changes in the spatial patterns of coseismic deformation during Holocene plate boundary earthquakes (Table 5).

	EQ9	EQ8	EQ7	EQ6	EQ5	EQ4	EQ3	EQ2	EQ1	1964	other	1964 obs
Yakataga								☑	☑			
Katalla						☑	☑	☑	☑	☑	☑	☑
Copper River Delta	☑	☑	☑	☑	☑	☑	☑	☑	☑	☑		☑
Portage				☑	☑	☑	☑	☑	☑	☑		☑
Girdwood				☑	☑	☑	☑	☑	☑	☑		☑
Bird Point						☑	☑	☑	☑	☑		☑
Anchorage								☑	☑	☑		☑
Kenai								☑		☑		☑
Kasilof								☑				☑
Homer				☑		☑	☑			☑		☑
Kodiak									☑	☑	☑	☑

Table 5: Comparison of paleoseismological evidence for coseismic surface deformation in 1964 and during 9 Holocene earthquakes. For ages of EQ1 through 6 see Shennan et al. (2014c) and Carver and Plafker (2008) for 7 through 9. The "other" column refers to earthquakes recorded at Katalla, ~500 BP (Shennan et al., 2014c) and in Kodiak ~500 BP and AD 1877 (Shennan et al., 2014a).

- *Tick indicates stratigraphic and age evidence present, unshaded for deformation most likely similar to that in 1964;*
- *red for deformation most likely greater than in 1964;*
- *brown where evidence for coseismic deformation is equivocal and if occurring is most likely less than in 1964.*
- *Gold with no tick indicates no evidence for coseismic deformation present in the stratigraphy.*
- *Grey indicates no sediment present of required age.*

These results imply that no previous great earthquake showed, in detail, the same spatial pattern of deformation as 1964. In two events the zone of uplift extend east into the Yakutaga segment (Shennan et al., 2009). Along the west coast of Kenai Peninsula EQ2 produced more subsidence than in 1964, whereas all the other prehistoric earthquakes produced limited or no evidence of coseismic deformation, at Kenai, Kasilof and Homer.

2.4 Research Question 4. Are great earthquake ruptures in Alaska controlled by persistent segment boundaries or do the rupture areas overlap?

The results outlined in sections 3.1 and 3.3 demonstrate that we cannot confirm that the segmentation model for the 1964 earthquake applies to previous great earthquakes. It is widely accepted that there were two main asperities in 1964, Prince William Sound and Kodiak (Figure 25A-C), but paleoseismic studies vary in how the segment boundaries persist through multiple earthquake cycles.

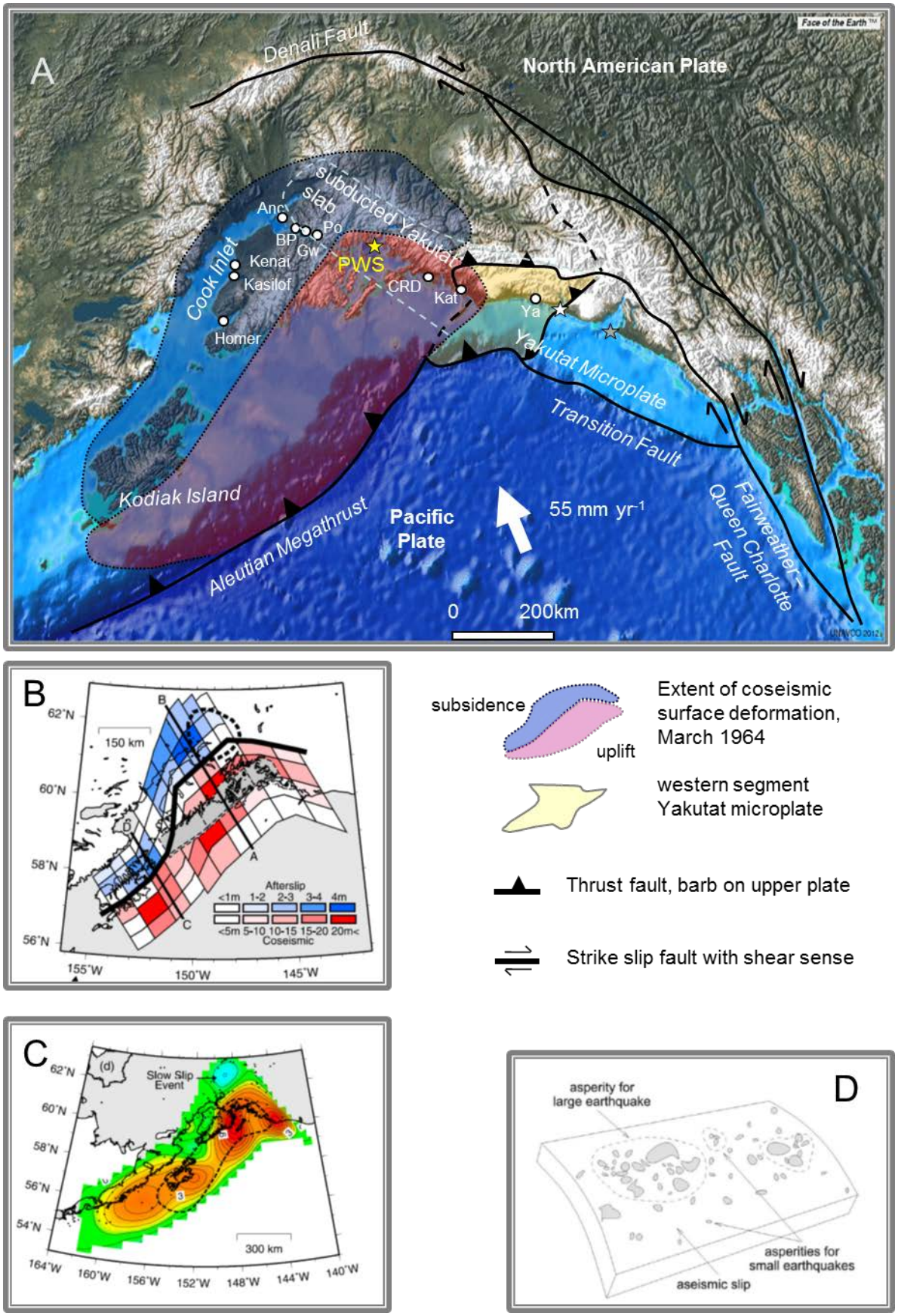

Figure 25: (A) Tectonic setting, extent of coseismic uplift and subsidence in 1964 and paleoseismic sites discussed in section 3.3. (B) Coseismic and post-seismic slip distributions for the 1964 earthquake (Suito and Freymueller, 2009). (C) Present day slip deficit distribution (Suito and Freymueller, 2009). (D) Conceptual asperity model of Wang (2007) in which the subduction fault is a mosaic of stronger and

weaker patches at all scales. Closely spaced stronger patches (asperities or groups of asperities) may form a larger asperity. Sparsely spaced asperities or groups of asperities may cause repeating earthquakes.

Some studies suggest two segments, a Kodiak segment and a Prince William Sound segment (Carver and Plafker, 2008; Nishenko and Jacob, 1990), and others suggest three, to include a central segment in the region of the Kenai Peninsula (Hutchinson and Crowell, 2007; Pulpan and Frohlich, 1985). While comprehensive, long records, 2000 years or more, only come from sites within the Prince William Sound segment (Figure 25A and Table 5) it remains difficult to test these segmentation models rigorously. Paleoseismic studies on Kodiak Island (Shennan et al., 2014a) and Sitkinak Island (Briggs et al., 2014) both provide evidence of rupture patterns that differ from those observed for 20th century earthquakes. Differences in the amount and spatial extent of coseismic submergence within the upper Cook Inlet part of the Prince William Sound segment (Hamilton et al., 2005; Shennan and Hamilton, 2006) may reflect variations in the down-dip extent of slip during past earthquakes. The records from Kenai (Hamilton and Shennan, 2005b) and those from Kasilof and Homer presented in this report, probably indicate that spatial variations in the present-day slip deficit distribution (e.g. figure 25C) in some way relate to characteristics of the subduction fault that impact through the coseismic and interseismic phases of multiple earthquake cycles. Wang (2007) offers a conceptual framework to investigate this (e.g. figure 25D). We should consider whether the patterns of coseismic deformation highlighted in table 5 reflect a mosaic of stronger and weaker patches. For example, the Prince William Sound segment would be an area of closely placed stronger patches, with the subduction interface characterised by the flat slab subduction of the Yakutat slab. Kenai, Kasilof and Homer would lie in a region of more widely spaced asperities and areas of aseismic slip; and Kodiak would be another area of closely spaced stronger patches.

3 Conclusions

We addressed the four research questions set out in the proposal and highlight six main conclusions.

(1) Of the five sites sampled, the most comprehensive records of relative land and sea-level changes come from Beluga Slough, Homer, with a >4000 year record, and Kasilof, a >6000 year record.
(2) Few of the peat-mud couplets at these sites fulfil the criteria for recording coseismic deformation.
(3) No previous great earthquake in the last few thousand years showed the same spatial pattern of deformation as 1964.
(4) Along the west coast of the Kenai Peninsula, a great earthquake c. 1500BP produced more subsidence than in 1964, whereas all the other prehistoric earthquakes produced limited or no evidence of coseismic deformation at Kenai, Kasilof and Homer.
(5) We find no evidence for tsunami deposits at Homer and Kasilof.
(6) Evidence from Kenai, Kasilof and Homer suggest that spatial variations seen in the present-day slip deficit distribution in some way relate to characteristics of the subduction fault that impact through the coseismic and interseismic phases of multiple earthquake cycles. This requires further analysis of new conceptual models about the pattern of asperities and areas of aseismic slip.

Acknowledgements: Pippa Whitehouse, Rod Combellick, Dick Reger and Chris Mayo – fieldwork and discussions; Catherine Kelham – additional diatom analyses.

4 References

Barlow, N.L.M., Shennan, I., Long, A.J., Gehrels, W.R., Saher, M.H., Woodroffe, S.A. and Hillier, C., 2013. Salt marshes as late Holocene tide gauges. Global and Planetary Change, 106(0): 90-110.

Begét, J., Gardner, C. and Davis, K., 2008. Volcanic tsunamis and prehistoric cultural transitions in Cook Inlet, Alaska. Journal of Volcanology and Geothermal Research, 176(3): 377-386.

Briggs, R.W., Engelhart, S.E., Nelson, A.R., Dura, T., Kemp, A.C., Haeussler, P.J., Corbett, D.R., Angster, S.J. and Bradley, L.-A., 2014. Uplift and subsidence reveal a nonpersistent megathrust rupture boundary (Sitkinak Island, Alaska). Geophysical Research Letters: 2014GL059380.

Carver, G. and Plafker, G., 2008. Paleoseismicity and Neotectonics of the Aleutian Subduction Zone - An Overview. In: J.T. Freymueller, P.J. Haeussler, R. Wesson and G. Ekstrom (Editors), Active tectonics and seismic potential of Alaska. Geophysical Monograph Series. American Geophysical Union, Washington, pp. 43-63.

Combellick, R.A. and Reger, R.D., 1994. Sedimentological and radiocarbon age data for tidal marshes along eastern and upper Cook Inlet, Alaska. Alaska Division of Geological and Geophysical Surveys Report of Investigations, 94-6: 1-60.

Hamilton, S. and Shennan, I., 2005a. Late Holocene relative sea-level changes and the earthquake deformation cycle around upper Cook Inlet, Alaska. Quaternary Science Reviews, 24(12-13): 1479-1498.

Hamilton, S., Shennan, I., Combellick, R., Mulholland, J. and Noble, C., 2005. Evidence for two great earthquakes at Anchorage, Alaska and implications for multiple great earthquakes through the Holocene. Quaternary Science Reviews, 24(18-19): 2050-2068.

Hamilton, S.L., 2003. Late Holocene relative sea-level changes and earthquakes around the upper Cook Inlet, Alaska, USA, Durham University.

Hamilton, S.L. and Shennan, I., 2005b. Late Holocene great earthquakes and relative sea-level change at Kenai, southern Alaska. Journal of Quaternary Science, 20(2): 95-111.

Hutchinson, I. and Crowell, A.L., 2007. Recurrence and Extent of Great Earthquakes in Southern Alaska During the Late Holocene from an Analysis of the Radiocarbon Record of Land-Level Change and Village Abandonment. Radiocarbon, 49(3): 1323-1385.

Nelson, A.R., Jennings, A.E. and Kashima, K., 1996. An earthquake history derived from stratigraphic and microfossil evidence of relative sea-level change at Coos Bay, southern coastal Oregon. Geological Society of America Bulletin, 108: 141-154.

Nishenko, S.P. and Jacob, K.H., 1990. Seismic potential of the Queen Charlotte - Alaska - Aleutian seismic zone. Journal of Geophysical Research, 95: 2511-2532.

Plafker, G., 1969. Tectonics of the March 27, 1964, Alaska earthquake. U.S. Geological Survey Professional Paper, 543-I: 74.

Pulpan, H. and Frohlich, C., 1985. Geometry of the subducted plate near Kodiak Island and Lower Cook Inlet, Alaska, determined from relocated earthquake hypocenters. Bulletin of the Seismological Society of America, 75(3): 791-810.

Reger, R.D., Sturmann, A.G., Berg, E.E. and Burns, P.A.C., 2007. A guide to the late Quaternary history of northern and western Kenai Peninsula, Alaska. State of Alaska Department of Natural Resources, Division of Geological & Geophysical Surveys Guidebook, 8: 1-112.

Shennan, I., Barlow, N., Carver, G., Davies, F., Garrett, E. and Hocking, E., 2014a. Great tsunamigenic earthquakes during the past 1000 yr on the Alaska megathrust. Geology, 42(8): 687-690.

Shennan, I., Barlow, N.L.M., Combellick, R., Pierre, K. and Stuart-Taylor, O., 2014b. Late Holocene paleoseismology of a site in the region of maximum subsidence during the 1964 Mw 9.2 Alaska earthquake. Journal of Quaternary Science, 29(4): 343-350.

Shennan, I., Bruhn, R., Barlow, N., Good, K. and Hocking, E., 2014c. Late Holocene great earthquakes in the eastern part of the Aleutian megathrust. Quaternary Science Reviews, 84: 86-97.

Shennan, I., Bruhn, R. and Plafker, G., 2009. Multi-segment earthquakes and tsunami potential of the Aleutian megathrust. Quaternary Science Reviews, 28(1-2): 7-13.

Shennan, I. and Hamilton, S., 2006. Coseismic and pre-seismic subsidence associated with great earthquakes in Alaska. Quaternary Science Reviews, 25(1-2): 1-8.

Suito, H. and Freymueller, J.T., 2009. A viscoelastic and afterslip postseismic deformation model for the 1964 Alaska earthquake. Journal of Geophysical Research: Solid Earth, 114(B11): B11404.

Wang, K., 2007. Elastic and viscoelastic models of subduction earthquake cycles. In: T.H. Dixon and J.C. Moore (Editors), The Seismogenic Zone of Subduction Thrust Faults. Columbia University Press, New York, pp. 540-575.

Watcham, E.P., Shennan, I. and Barlow, N.L.M., 2013. Scale considerations in using diatoms as indicators of sea-level change: lessons from Alaska. Journal of Quaternary Science, 28(2): 165-179.

Waythomas, C.F., 2000. Reevaluation of Tsunami Formation by Debris Avalanche at Augustine Volcano, Alaska. pure and applied geophysics, 157(6-8): 1145-1188.